Cu-Ga^{3+}-doped wurtzite ZnO interface as driving force for enhanced methanol production in co-precipitated Cu/ZnO/Ga$_2$O$_3$ catalysts

Jorge Cored [a], Christian Wittee Lopes [a,1], Lichen Liu [a,2], Jose Soriano [a], Giovanni Agostini [b], Benjamín Solsona [c], Rita Sánchez-Tovar [c], Patricia Concepción [a,*]

[a] Instituto de Tecnología Química, Universitat Politècnica de València-Consejo Superior de Investigaciones Científicas (UPV-CSIC), Avenida de los Naranjos s/n, 46022 Valencia, Spain
[b] CELLS – ALBA Synchrotron Radiation Facility, Carrer de la Llum 2-26, 08290 Cerdanyola del Vallès, Spain
[c] Department of Chemical Engineering, Universitat de València, Av. Universitat s/n, 46100 Burjassot, Spain

ARTICLE INFO

ABSTRACT

A detailed understanding of the interactions among the active components in gallium promoted Cu/ZnO catalysts, depending on the speciation of the gallium, are reported using in situ/operando spectroscopic studies, and their effect in the CO$_2$ hydrogenation to methanol unraveled. In this contribution, the promoting effect of Ga^{3+}-doped in the wurtzite ZnO lattice of a Cu/ZnO/Ga$_2$O$_3$ catalyst is compared to that of a zinc gallate (ZnGa$_2$O$_4$) phase. Remarkably, a strong inhibition of CO formation, together with an enhanced methanol formation, are observed in the Ga^{3+}-doped ZnO sample, specifically at conditions where the competitive reverse water gas shift reaction predominates. The catalytic performance has been correlated with the microstructure of the catalyst where a surface enrichment with reduced ZnO$_x$ species, together with the stabilization of positive charged copper species and an increase in the amount of surface basic sites for CO$_2$ adsorption are observed on the most selective sample.

© 2022 The Author(s). Published by Elsevier Inc. This is an open access article under the CC BY-NC-ND license (http://creativecommons.org/licenses/by-nc-nd/4.0/).

1. Introduction

Methanol is one of the most important feedstocks in the chemical industry and represents a promising energetic vector for a sustainable economy with an annual production of about 95 million tonnes [1]. Currently, almost all methanol is produced from fossil fuels, i.e., natural gas and coal. Industrial methanol synthesis catalysts are bulk systems composed of strongly interacted Cu and ZnO nanoparticles as functional components, and 5–10 mol% Al$_2$O$_3$ as a structural promoter to improve the dispersion of copper and the catalyśt́s thermal stability. In the last years, environmental concerns due to the increased emission of CO$_2$ and its adverse effect in our planet has attracted much attention toward the capture and use of CO$_2$ for the production of chemicals and fuels, coupled with the integration of renewable energy. In this sense, the synthesis of methanol using CO$_2$ as feedstock and H$_2$ generated from renewable energy represents a sustainable and promising way for CO$_2$ recycling and hydrogen storage [2]. The performance of the current commercial Cu/ZnO/Al$_2$O$_3$ methanol catalyst is not sat-

isfactory for the CO$_2$ hydrogenation reaction, giving low methanol yields due to thermodynamic limitations and the competitive reverse water gas shift reaction (RWGS), as well as serious catalyst deactivation issues because of the sintering of the copper and ZnO components in the presence of water as by-product [3]. Thus, the development of highly active, selective and stable catalysts remains a challenge. Extensive studies including new catalyst developments, fundamental understanding of the nature of the active sites, optimization of the reaction conditions and reactor designs have been demonstrated in numerous reviews and publications [4–7]. In this direction, different models of active sites are proposed in the literature, where the presence of metal-support interfacial sites are believed to play a key role in the methanol synthesis reaction [8]. In addition, many studies are focused on the structural parameters of the Cu species, such as particle size, exposed crystal facets, defects and lattice strains [9]; formation of CuZn alloys [10,11]; stabilization of Cu$^+$ sites and migration of ZnO$_x$ on the copper surface and the formation of surface vacancies for stabilization of intermediate species [12–16]. The addition of promoters to improve the catalytic performance of commercial-like catalysts has been widely reported, and among them, Ga^{3+} has emerged as a promising candidate [10,11,14,17]. The promoting effect depends on the speciation of Ga^{3+} in the final catalyst, which is influenced by the synthetic conditions. Thus,

---

some authors suggest that the promoting effect of Ga depends on the size of the Ga_2O_3 nanoparticles, in the sense that the presence of highly dispersed Ga_2O_3 particles favours the formation of Cu^+ species [14,15]. Other authors reported the formation of a $ZnGa_2O_4$ spinel phase, which creates an electronic heterojunction with excess of ZnO, facilitating the reduction of ZnO to Zn^0 [9–11]. Reduced Zn adatoms migrate and decorate step sites in the Cu NP, resulting in CuZn alloy species. Other authors found that the addition of gallium generates new active sites, where the adsorption energies of intermediate species are modified, decreasing the apparent activation energy for methanol formation, but not for the RWGS [18]. In other studies, more than behaving as a structural promoter, an electronic promoting effect of Ga^{3+} has been reported, in analogy to that observed in Al-promoted Cu/ZnO catalysts at low Al^{3+} concentrations (<3.5 wt%) [19]. In that work, the partial substitution of Zn^{2+} with Al^{3+} and their effect on the redox and structural properties of the catalyst has been studied and extrapolated to Ga^{3+} and Cr^{3+}.

The doping of ZnO with other elements such as N^{3+}, Al^{3+}, In^{3+} or Ga^{3+} has attracted great interest in the field of optoelectronics as a way of modulating the conductivity of ZnO as n-type semiconductor. In this direction, the role of Ga^{3+} doped in the ZnO wurtzite structure has sustained great expectatives in electronic devices [20,21]. In line with these works, the goal of our study is to explore the doping effect of ZnO with Ga^{3+} in the methanol synthesis from CO_2 hydrogenation, working on complex commercial-like Cu/ZnO/Ga_2O_3 systems. To our knowledge, Ga^{3+}-doped wurtzite ZnO copper-based catalysts has scarcely been studied in the literature. Combining catalytic studies with in situ/operando characterization techniques, a detailed understanding of the structural, electronic and catalytic promoting effects of Ga^{3+} doped in the ZnO lattice of a Cu/ZnO/Ga_2O_3 sample, compared to that of a zinc gallate ($ZnGa_2O_4$) phase, has been obtained. Interestingly, the interface between copper and Ga-doped ZnO was identified as the driving force for enhanced methanol selectivity, paving the way to a rational design of new highly efficient catalysts.

2. Materials and methods

Synthesis of CZG-sp and CZG-ox (CuO/ZnO/Ga_2O_3). Catalysts were prepared by co-precipitation method. In particular, for a CuO/ZnO/Ga_2O_3 chemical composition of 70: 24: 6 (Cu: Zn: Ga wt% ratio); Cu(NO$_3$)$_2$·2.5H$_2$O (7.90 g, Sigma Aldrich, >98%), Zn (NO$_3$)$_2$·6H$_2$O (3.69 g, Fluka, >99%) and Ga(NO$_3$)$_3$·xH$_2$O (0.26 g, Alfa Aesar, 99.9%) metallic precursors dissolved in deionized water (41.99 g) were pumped at 0.5 mL·min^{-1} (kd Scientific, KDS-200 syringe pump) to a round bottom flask containing 200 mL of deionized water at 65 °C and under stirring. Simultaneously, a 1.4 M basic solution of a precipitating agent (∼80 mL) was pipetted to the flask in order to keep the pH constant at 6.5. In detail, NH$_4$HCO$_3$ (Aldrich, 99.5%) and NaOH (Scharlab, >98%) aqueous solutions were used to synthesize CZG-sp and CZG-ox samples, respectively. Then, the suspension was aged under stirring at 65 °C for 2 h. Afterwards, the precipitate was filtered, washed with hot deionized water until pH = 7 and dried overnight at 100 °C to yield a coloured solid (4.98 g, turquoise for CZG-sp; 3.39 g, dark brown for CZG-ox). The resulting solid was calcined in a muffle furnace as follows: from 25 °C to 200 °C (2 °C·min^{-1}; dwell time: 1 h), from 200 °C to 360 °C (2 °C·min^{-1}; dwell time: 1 h), and finally kept at 360 °C for 9.5 h. After calcination, a dark solid was obtained (3.78 g for CZG-sp; 3.22 g for CZG-ox). Synthesis of CZG-ox samples at variable gallium loadings and CZGA-ox catalyst with a 12 wt% Al_2O_3 are described in SI. The scalable approach of the synthesis has been studied preparing two additional batches by doubling

(6.48 g) and tripling (9.61 g) the final yield. Details of the synthesis are given in the SI.

Synthesis of CZA (Cu/ZnO/Al_2O_3). Catalyst was prepared by a co-precipitation method following the procedure reported by Baltes et al. [22] Synthetic details are found in SI.

ZnO (Aldrich, 99.9%) and Ga_2O_3 (Aldrich, 99.99+%) were used as reference samples in characterization studies.

Metallic content (Cu, Zn, Ga, Al) was analysed by Inductively Coupled Plasma Optical Emission Spectrometry (ICP-OES) using a Varian 715-ES spectrometer after solid dissolution of catalysts in HNO$_3$/HCl aqueous solution.

X-Ray powder diffraction (XRD) was recorded with a PANalytical Cubix Pro diffractometer using a monochromatic Cu K$_\alpha$ radiation (λ = 0.15406 nm). Average Cu^0 crystallite size (JCPDS: 01-070-3038) was calculated from the main peaks (43.1, 50.2, 73.9; 2θ) using the Scherrer equation and assuming a shape factor k = 0.9.

Surface areas of solid samples (250 mg) were calculated by applying the Brunauer-Emmett-Teller (BET) model to the range of the N_2 adsorption isotherm where a linear relationship is maintained. These isotherms were obtained from liquid nitrogen adsorption experiments at −196 °C, in a Micromeritics flowsorb instrument.

Transmission Electron Microscopy (TEM) measurements were performed in a JEOL-JEM 2100F operating at 200 kV. Samples were prepared by dropping the suspension of the powder catalyst using ethanol as the solvent directly onto holey-carbon coated copper grids.

The amount of surface copper metal sites was measured by N_2O surface oxidation [23] followed by Temperature Programmed Reduction with H_2 (TPR-H_2) in a Micromeritics Autochem 2910 instrument, assuming an adsorption stoichiometry of 1:2 (H_2: Cu_s). Before measurements, about 50 mg of catalyst was activated in 20 mL·min^{-1} H_2 flow (pure H_2, 3 h, 200 °C for CZG samples; 10 vol% H_2 in Ar, 1 h, 200 °C for CZA). After reduction, the sample was cleaning at the same temperature under argon flow. The temperature was decreased to 25 °C and the surface oxidation using N_2O (1 vol% in He, 10 mL·min^{-1}) was performed for 1 h. After the first treatment, the sample was flushed with argon (15 min) at room temperature. Finally, TPR-H_2 was submitted until 400 °C (10 vol% H_2 in Ar, 50 mL·min^{-1}, 10 °C·min^{-1}).

Electrochemical measurements. Electrochemical Impedance Spectroscopy (EIS) tests were performed in a three electrode electrochemical cell connected to a potentiostat using the catalyst as working electrode (with an exposed area to the electrolyte of 0.5 cm^2), an Ag/AgCl (3 M, KCl) reference electrode and a platinum tip as counter electrode. The working electrode was made by the deposition of 30 mg of ex situ reduced catalyst dispersed on 0.5 mL of ethanol on a FTO glass. The deposition was carried out using a spin coating at 3000 rpm. EIS were carried out at 0 $V_{Ag/AgCl}$ and applying a potential perturbation of 10 mV from 10 kHz to 10 mHz. Additionally, Mott-Schottky plots were conducted scanning the potential from 0.2 V to −1.0 $V_{Ag/AgCl}$ at a rate of 50 mV s^{-1} at 5000 Hz. The electrolyte used for the electrochemical measurements was 0.1 M Na_2SO_4.

Temperature Programmed Desorption (TPD-CO_2) studies over *in situ* reduced samples were performed using a quartz reactor, connected online to a mass spectrometer (MS) Balzer (QMG 220 M1). 100 mg of sample was firstly activated in a 20 mL·min^{-1} H_2 flow at 200 °C for 3 h (1 h and 10 vol% H_2 in Ar for CZA sample, pure H_2 for the others). Then, the sample was flushed with argon (18 mL·min^{-1}) at 230 °C for 1 h and the temperature decreased to RT. After stabilization, CO_2 was pulsed 15 times using a four way-valve (100 μL loop). After the adsorption step, the temperature was increased to 650 °C, maintaining the inert flow (10 °-C·min^{-1}). CO_2 desorption was followed by MS (m/z = 44).

Hydrogen/Deuterium (H/D) exchange experiments were carried out in a flow reactor at 25 and 90 °C. The feed gas consisted of 4 mL·min^{-1} H$_2$, 4 mL·min^{-1} D$_2$ and 18 mL·min^{-1} argon, and the total weight of catalyst was 41 mg. The sample was diluted with 360 mg of SiC. Reaction products (H$_2$, HD and D$_2$) were analysed with a mass spectrometer (Omnistar, Balzers). The m/z values used were 2 (H$_2$), 4 (D$_2$) and 3 (HD). The sample was *in situ* reduced at 200 °C (10 mL·min^{-1}; 100 vol% H$_2$, 3 h for CZG-sp and CZG-ox; 10 vol% H$_2$ in Ar, 1 h, for CZA) with a temperature-rising rate of 10 °C·min^{-1}. Then, the temperature was decreased to 25 °C and, once stabilized, the H$_2$ feed was changed to the reactant gas composition. The temperature was kept at 25 °C for about 60 min and then, increased to 90 °C maintaining 60 min at that temperature.

Infrared (IR) spectra were recorded with a Nicolet (Nexus) 8700 FTIR spectrometer using a DTGS detector and acquiring at 4 cm^{-1} resolution. An IR cell allowing *in situ* treatments in controlled atmospheres and temperatures from −176 °C to 500 °C was connected to a vacuum system with gas dosing facility. For IR studies, samples were pressed into self-supported wafers and submitted to hydrogen atmosphere prior to CO titration. For the reduction studies, CZG-sp, CZG-ox and CZA samples were treated at 200 °C in H$_2$ flow (10 mL·min^{-1}; 100 vol% H$_2$, 3 h for CZG-sp and CZG-ox; 10 vol% H$_2$ in N$_2$, 1 h, for CZA) followed by evacuation at 10^{-4} mbar at the same temperature for 1 h and cooling down to −50 °C under dynamic vacuum conditions. CO was dosed at −50 °C and at increasing pressure (2–18 mbar). IR spectra were recorded after each dosage.

X-ray absorption experiments at the Cu (8979 eV) and Zn (9659 eV) K-edges were performed at the BL22 (CLÆSS) beamline [24] of ALBA synchrotron (Cerdanyola del Vallès, Spain). The white beam was monochromatized using a Si(111) double crystal; harmonic rejection was performed using Rh-coated silicon mirrors. Spectra were collected in transmission mode by means of the ionization chambers filled with appropriate gases. Samples in the form of self-supported pellets of optimized thickness have been located inside in-house built cells allowing *in situ* experiments. Several scans were acquired at each measurement step to ensure spectral reproducibility and a good signal-to-noise ratio. The data reduction and extraction of the χ(k) function as well as the EXAFS data analysis have been performed using the Demeter package [25]. Phase and amplitudes have been calculated by FEFF6 code.

Near ambient pressure X-ray photoelectron spectroscopy (NAP)-XPS experiments were performed at ISISS beamline (HZB/Bessy II Electron Storage Ring, Berlin, Germany), where the photon energy range is 80–2000 eV. The endstation is equipped with a Petersen-type plane grating monochromator (PGM). Data were acquired with a Phoibos HSA 3500 electron energy analyzer (SPECS GmbH), pass energy of 20 eV, a step of 0.1 eV and beamline exit slit of 111 μm. The focus size was 100 × 80 (HxV) μm^2. Incident photon energies of 1200, 1290, 1386 and 1600 eV for Cu 2p$_{3/2}$; 1200, 1290 and 1600 eV for Zn 2p$_{3/2}$; 1290, 1386 and 1600 eV for Ga 2p$_{3/2}$; 1200 and 1386 eV for Cu LVV AES and 700 eV for O 1s were used, allowing to probe sample depths between 2.0 and 4.3 nm. The probing depth was obtained using the Tanuma Powell and Penn algorithm (TPP2M), calculating the inelastic mean free path for ZnO model [26]. The sample (~30 mg) was pelletized, mounted onto a sapphire sample holder and transferred directly to the analysis chamber with an insertion tool. Gas mixtures for the *in situ* experiments were set in a proper ratio adjusting various mass flow controllers (Bronkhorst) present in a gas manifold that was directly connected to the analysis chamber through a leak valve. CZG-sp, CZG-ox and CZA samples were reduced *in situ* before performing CO$_2$ hydrogenation reaction. For that purpose, constant pressure of 0.5 mbar H$_2$ (10 mL·min^{-1}) was kept in the chamber and the temperature raised from 25 to 200 °C (2 °C·min^{-1}) for a total reduction time of ~2 h. After the complete reduction of copper,

the atmosphere was switched to a 2.5 mbar gas mixture of CO$_2$ and H$_2$ (1:3 mol ratio, 12 mL·min^{-1}) to perform the CO$_2$ hydrogenation reaction. XPS data were acquired under reaction conditions at 220 °C (~5–7 h) and at 280 °C (~3–4 h). Products evolution was monitored using a Prisma Balzers Mass Spectrometer, which was connected to the chamber via a leak valve. The m/z values used in the identification were: 32 (MeOH), 2 (H$_2$), 18 (H$_2$O), 44 (CO$_2$) and 28 (CO). The energy scales of the XPS spectra were calibrated using the Fermi edge position. The (NAP)-XPS data were analysed using CASA XPS software. Shirley type background and Gaussian/Lorentzian type curves have been used in the spectra fitting.

CO$_2$ hydrogenation catalytic studies were performed in a stainless steel fixed bed reactor (inner diameter of 11 mm and 240 mm length), equipped with a back pressure regulator (BPR, Swagelok) that allows for working at a pressure range of 1–20 bar. Typically, 180 mg of catalyst (particle size 400–600 μm) was diluted in SiC in a weight ratio 0.12 (Cat/SiC). Samples were *in situ* reduced at atmospheric pressure prior to catalytic tests (25 mL·min^{-1} H$_2$, 200 °C, 3 h, 10 °C·min^{-1} for CZG samples; 25 mL·min^{-1} with 10 vol% H$_2$ in N$_2$, 200 °C, 1 h, 10 °C·min^{-1}, for CZA sample). Experiments at constant weight hourly space velocity (WHSV, ~31000 mL·g$_{cat}^{-1}$·h^{-1}) were performed under concentrated reaction conditions (23.7 vol% CO$_2$, 71.3 vol% H$_2$, 5.0 vol% N$_2$) at 20 and 1 bar. Reaction temperatures varied from 160 to 260 °C. Each temperature was maintained for at least 1.5 h. Catalytic experiments at variable WHSV (~24000–134000 mL·g$_{cat}^{-1}$·h^{-1}) were carried out at constant 3:1 H$_2$ to CO$_2$ mol ratio and 20 bar. Long-term experiments were conducted at 240 °C and 20 bar over 100 h at constant WHSV (28500 mL·g$_{cat}^{-1}$·h^{-1}) and under the concentrated conditions described above. Direct analysis of the reaction products was done by online gas chromatography (GC), using a SCION-456-GC equipment with TCD (MS-13X column) and FID (BR-Q Plot column) detectors. Blank experiments (in the presence of SiC) shown the absence of a homogeneous contribution to the reaction. Intrinsic activity (expressed as mol$_{product}$·mol$_{Cu,s}^{-1}$·s^{-1}) was calculated through the number of copper exposed sites obtained by N$_2$O copper surface oxidation followed by TPR-H$_2$ studies (see above).

3. Results and discussion

3.1. Synthesis and physico-chemical properties of calcined and reduced catalysts

The importance of synthetic conditions in the stabilization of different crystalline precursor phases influencing the structure of the final catalyst has been reported in many works [4]. Commercial-like Cu/ZnO catalysts are usually prepared by coprecipitation of the metal precursors using carbonates (Na$_2$CO$_3$, NH$_4$-HCO$_3$) as precipitating agent at controlled pH (~6.5), resulting in the formation of zinc malachite, aurichalcite or hydrotalcite precursor phases [10,27]. With the addition of other cations like Al^{3+} or Ga^{3+}, the composition of the precursor phases may change. In this direction, Tsang et al. disclosed the formation of a ZnGa$_2$O$_4$ spinel phase in coexistence with ZnO, introducing 5–20 mol% Ga^{3+} into a Cu/ZnO precursor mixture, coprecipitated in the presence Na$_2$CO$_3$.[10] In contrast, the doping of ZnO with other elements such as Al^{3+}, Ga^{3+}or Cr^{3+} has been shown critical if a carbonate route is used, being strongly dependent on the synthesis conditions [19]. Therefore, an alternative precipitation route in absence of carbonates, i.e., using NaOH, has been selected in our work.

Thus, two CuO/ZnO/Ga$_2$O$_3$ catalysts are prepared by a coprecipitation method at controlled pH and in the presence of different precipitation agents (ammonium hydrogen carbonate for the CZG-sp sample and sodium hydroxide for the CZG-ox sample)

(see details in Experimental Section). In the first case, zincian malachite is formed in the as-precipitated sample, whereas in the second case, wurtzite ZnO and CuO are formed (details in SI). The composition of the CuO/ZnO/Ga$_2$O$_3$ catalysts has been settled similar to that of commercial-like CuO/ZnO/Al$_2$O$_3$ catalysts (i.e., 70: 24: 6 wt% ratio for Cu, Zn and Ga or Al) [22,28]. After calcination in air at 360 °C, the samples were reduced in H$_2$ (25 mL·min^{-1}) at 200 °C for 3 h. For comparative purposes, a commercial-like catalyst (Cu/ZnO/Al$_2$O$_3$, labelled as CZA) with identical chemical composition has been prepared using a procedure described in the literature [22] (details in SI).

The structural properties of the reduced catalysts were analysed by XRD and X-ray absorption spectroscopy (XAS) at the Cu and Zn K-edges, where the identification of ZnO and Cu^0 are confirmed in all samples (SI). Meanwhile, diffraction peaks associated to any gallium phase are not detected in the XRD patterns, inferring for a high dispersion of the Ga species (Figs. S2–S5). In addition, according to the Scherrer equation the average particle sizes of Cu^0 are in all samples above the threshold defined in the CO$_2$ hydrogenation for highest activity [29]. Thus, values of ~11 nm in the CZG-sp sample, ~17 nm in CZG-ox and ~9 nm in the CZA sample are obtained.

Regarding the speciation of the Ga species, X-ray absorption (XAS) spectroscopy at the Ga K-edge reveals a different local environment around Ga atoms in both CZG catalysts. Normalized XANES spectra at Ga K-edge (10367 eV) of CZG samples and Ga-based standards are shown in Fig. 1a, where all spectra show similar absorption edge positions (10372 eV), corresponding to Ga^{3+} compounds. CZG-ox displays a spectrum with a typical feature beyond the edge (10389 eV, marked with an arrow), which is attributed to Ga atoms involved in a wurtzite-type structure [30–32]. According to the chemical composition of our samples, the possible wurtzite structures prone to be formed are GaN or Ga^{3+}-doped ZnO phase (replacement of Zn^{2+} with Ga^{3+}). However, the performed chemical analysis ruled out the formation of GaN, then suggesting that Ga atoms are inserted into zinc oxide crystalline structure. This hypothesis is supported by the comparison made in the inset of Fig. 1a, in which both Ga and Zn K-edge spectra of CZG-ox are displayed with the same XANES features, which was already reported in the literature as proof of wurtzite structure formation. On the other hand, the CZG-sp catalyst showed a XANES spectrum quite similar to that of ZnGa$_2$O$_4$. A small undulation noticed before the marked ZnGa$_2$O$_4$ feature could be associated to a minor presence of Ga$_2$O$_3$ or even a percentage of Ga with wurtzite structure as in CZG-ox, once this shoulder lies at the same energy values. The k^2-weighted $\chi(k)$ functions and |FT| of Fig. 1b and c were useful to further support the features observed in XANES, despite the short k-space (2–7.5 Å^{-1}), which limits our discussion to the first oscillations and, consequently, qualitative first shell analysis. The $\chi(k)$ functions of CZG-sp and ZnGa$_2$O$_4$ present the same in-phase oscillations with higher intensities for the latter (due to its more crystalline character), which resulted in similar EXAFS spectra after applying the Fourier-transform. Conversely, the $\chi(k)$ functions of CZG-ox catalyst are rather different, especially in the 6.0–7.5 Å^{-1} range, corresponding to a Ga^{3+}-doped ZnO phase.

Analysis of the microstructure of the samples performed with high-resolution transmission electron microscopy (HRTEM) imaging shows the coexistence of domains with different composition in both gallium promoted samples. Thus, the integration of Cu (d$_{111}$ = 0.20 nm), ZnO (d$_{101}$ = 0.24 nm) and ZnGa$_2$O$_4$ (d$_{111}$ = 0.48 nm) phases, in close intimacy, are observed in the CZG-sp sample (Fig. 2a). Similar features of Cu and ZnO phases are observed in the CZG-ox sample (Fig. 2b), while the identification of the Ga^{3+}-doped ZnO phase was hardly visualized from HRTEM imaging because of the very small variation of the lattice

distance due to the Ga doping. From energy dispersive X-ray (EDS) mapping results, Ga overlaps with Zn in the CZG-ox sample (Fig. 2c), which could be related to the formation of the Ga^{3+}-doped ZnO phase in which the Ga species are present as dopants in the ZnO nanoparticles. In contrast, a more homogeneous distribution of all elements (Cu, Zn and Ga) is visualized in the EDS mapping of the CZG-sp sample (Fig. 2d).

The electronic properties of the samples have been proven by Electrochemical Impedance Spectroscopy (EIS) measurements. In particular, the total resistance of each catalyst can be obtained from the Bode-module plot reading the impedance module value at low frequencies (Fig. 3). As shown in Fig. 3, an increment in the conductivity (i.e., a decrease in the total resistances) of the Ga promoted samples (CZG-ox and CZG-sp) versus the un-doped commercial-like CZA is clearly observed. This can be explained in view of Al$_2$O$_3$ micro-structural role, where the aluminum phase is mainly acting as dispersing agent of the ZnO and Cu nanoparticles. In this sense, the electrical interparticle transport is hindered due to the isolating intrinsic properties of Al$_2$O$_3$.

In the case of Ga promoted samples, both show similar total electrical resistances, being slightly lower in the CZG-sp system, which indicates a higher amount of structural defects (according to N$_D$ values of Fig. S8: 4.92·10 [19] and 1.73·10 [19] cm^{-3} for the CZG-sp and CZG-ox samples, respectively). The low carrier mobility observed in the CZG-ox sample may be due to carrier compensation, where part of the Ga occupies interstitial sites as neutral defects [33]. Besides, an excess of Ga might form a low proportion of Ga$_2$O$_3$, while not detected spectroscopically, which could be somehow responsible for the higher total resistance value of the CZG-ox catalyst due to a reduction of the carrier density [33–35]. Additionally, the positive slope showed in the Mott-Schottky plots confirms the n-type semiconductor behaviour of the catalysts with oxygen vacancies and Zn^{2+} interstitials as main defects (Fig. S8).

*3.2. Catalytic activity in the CO$_2$ hydrogenation*

The catalytic performance of the Ga-promoted samples (CZG) and that of the commercial CZA sample, as reference, in the CO$_2$ hydrogenation at 20 bar and at a space velocity (WHSV) of ~31000 mL·g$_{cat}^{-1}$·h^{-1} is included in Table 1. The variation of the CO$_2$ conversion and the selectivity to products at different reaction temperatures are summarized in Fig. 4a–c.

Similar catalytic performance in terms of CO$_2$ conversion is observed for the CZG-sp and CZA samples, being these more active than the CZG-ox sample. Normalizing the samples production to MeOH and CO per gram of catalyst (STY), a comparable value is found for the former product at all the temperatures for the three catalysts (Table 1), however when the normalization is done to square meter of catalyst (Table S5a), a ~2 times higher methanol production is observed in the CZG-ox system. In addition, if the variation of the selectivity to the main product (i.e., MeOH) is plotted versus its productivity (Fig. 4d), a difference of 20 percentage points is found for the selectivity between the CZG-ox and the commercial CZA systems, and 15 points between the CZG-ox and CZG-sp samples. This trend suggests a strong inhibition of CO formation in the gallium promoted samples and, in particular, in the CZG-ox catalyst.

The same behaviour is also observed when plotting the variation of the selectivity to methanol with the CO$_2$ conversion obtained at different contact times. This is displayed in Fig. 5 at two temperatures (i.e., 220 °C and 240 °C) as examples, and the catalytic data included in Table S5 and Fig. S9.

In both graphs, a nearly parallel catalytic behaviour is found for the CZG and CZA systems, being the CZG-ox catalyst the most selective one at any operational condition. Thus, at 220 °C and
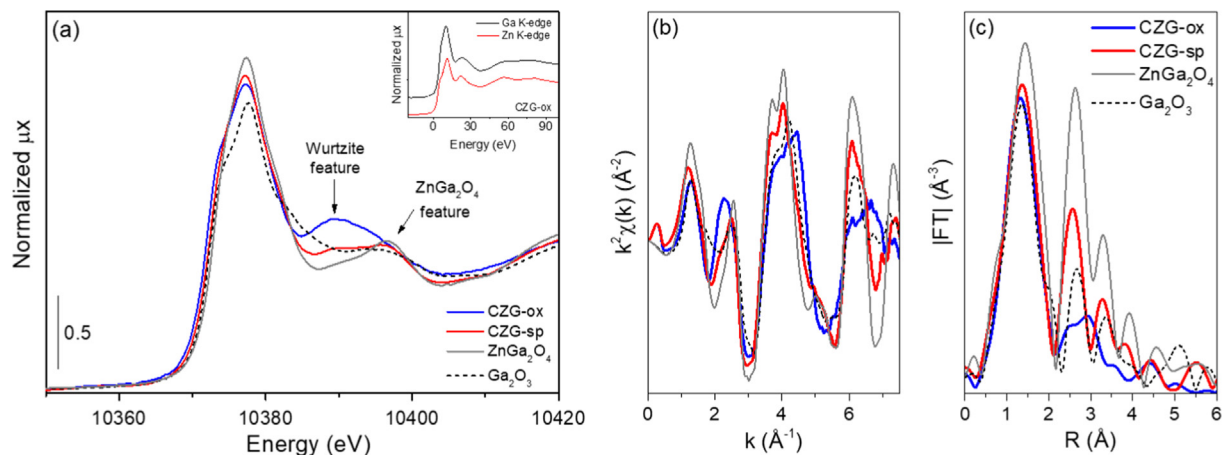
Fig. 1. Normalized XANES spectra at Ga K-edge (a), phase-uncorrected, k^2-weighted $\chi(k)$ functions (b) and EXAFS spectra (c) of CZG catalysts and Ga-based references. *Inset*: comparison of CZG-ox sample measured at Ga and Zn K-edges showing the similarity in XANES features, attributed in literature to wurtzite-type structures [31,32].
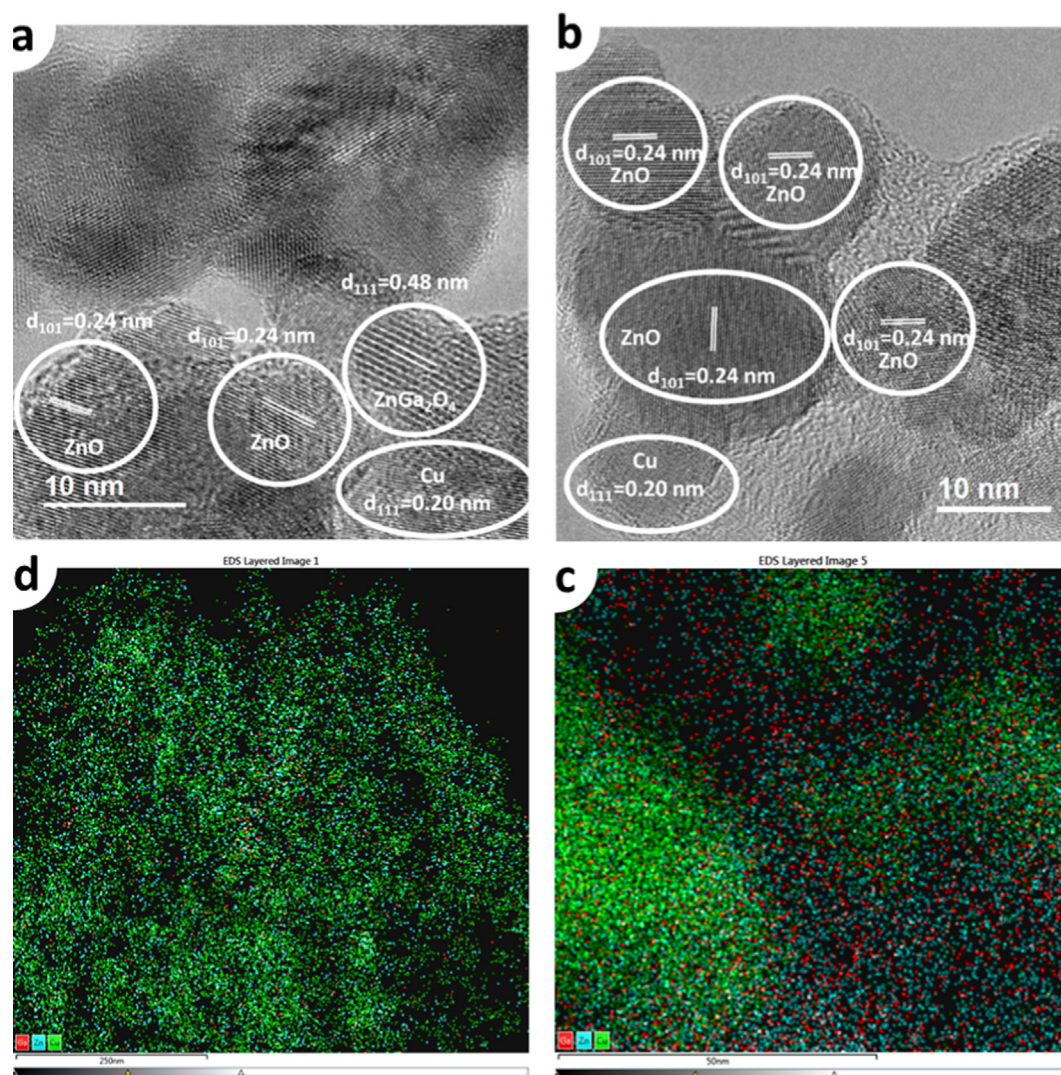
Fig. 2. Structural characterization of CZG-ox and CZG-sp samples. High-resolution transmission electron microscopy (HRTEM) images of CZG-sp (a) and CZG-ox (b) samples. The different components are marked according to the lattice fringes. STEM-EDS mapping results of CZG-ox (c) and CZG-sp (d). The Ga (red), Zn (cyan) and Cu (green) are indicated by different colours in the images. (For interpretation of the references to colour in this figure legend, the reader is referred to the web version of this article.)
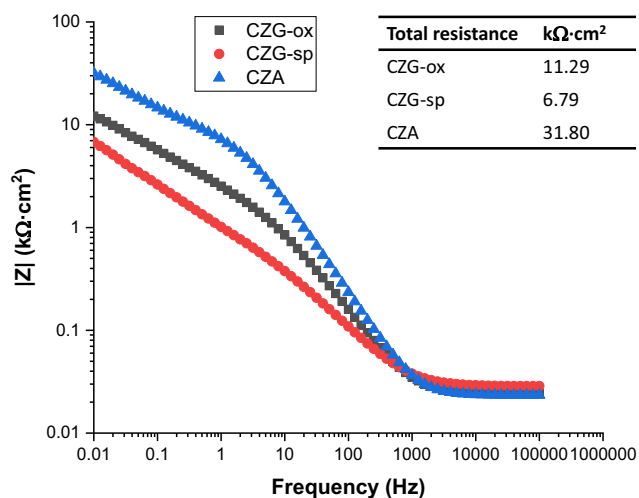
Fig. 3. Bode Module plot and total resistance values of the reduced CZG-ox, CZG-sp and CZA samples in 0.1 M Na_2SO_4 at 0 $V_{Ag/AgCl}$.

9.5% CO_2 conversion, a 89.0% methanol selectivity is obtained with the CZG-ox catalyst, being higher than the other two catalysts (85.5% with CZG-sp and 82.1% with CZA). The enhanced methanol selectivity is even more remarkable at higher temperatures, i.e., 260 °C (Fig. S10), at which the RWGS reaction becomes predominant. In this case, at a ~15.5% CO_2 conversion, a selectivity to methanol of 65.0% is achieved with the CZG-ox, being 9% and 16% points higher than those with the others samples (i.e., 56.2% and 49.0% with CZG-sp and CZA, respectively).

Due to the different amount of exposed copper atoms on the surface of the CZG and CZA samples (see Table S1), additional normalization of the catalytic activity to the exposed Cu surface area (SA_{Cu}, measured by N_2O chemisorption) is done for qualitative analysis, being aware of the controversy about the meaning of this value, particularly for reactions requiring the concertated involvement of metallic and oxide species. Interestingly, the intrinsic methanol activity is the highest for the CZG-ox sample ($6.99 \cdot 10^{-3}$ $mol_{MeOH} \cdot mol_{Cu,s}^{-1} \cdot s^{-1}$ at 240 °C), which is 2 times than that in the CZG-sp and CZA samples ($3.73 \cdot 10^{-3}$ $mol_{MeOH} \cdot mol_{Cu,s}^{-1} \cdot s^{-1}$ and $3.23 \cdot 10^{-3}$ $mol_{MeOH} \cdot mol_{Cu,s}^{-1} \cdot s^{-1}$, respectively). In summary, a promoting effect in methanol production can be concluded in the CZG-ox sample, compared to the commercial-like CZA and $ZnGa_2O_4$ containing CZG-sp samples.

In the next, in order to define the catalytic role of Ga^{3+} doped in the ZnO lattice of the CZG-ox sample, the performance of the herein studied catalysts has been compared to other gallium promoted catalysts from the literature. This is collected in Table S7, where the methanol production (i.e., STY) and its selectivity among different Ga promoted catalysts are compared. Comparison is complicated due to the usually diverse reaction conditions used in the literature, being methanol formation favoured at high pressures and high space velocities. However, despite these dissimilarities, analysing the methanol space time yields (STY_{MeOH}) at a selected temperature and contact time (Fig. S11), the herein reported catalysts appear among the most active ones, with the benefit of a lower working pressure, endowing as promising candidates in the CO_2 hydrogenation to methanol.
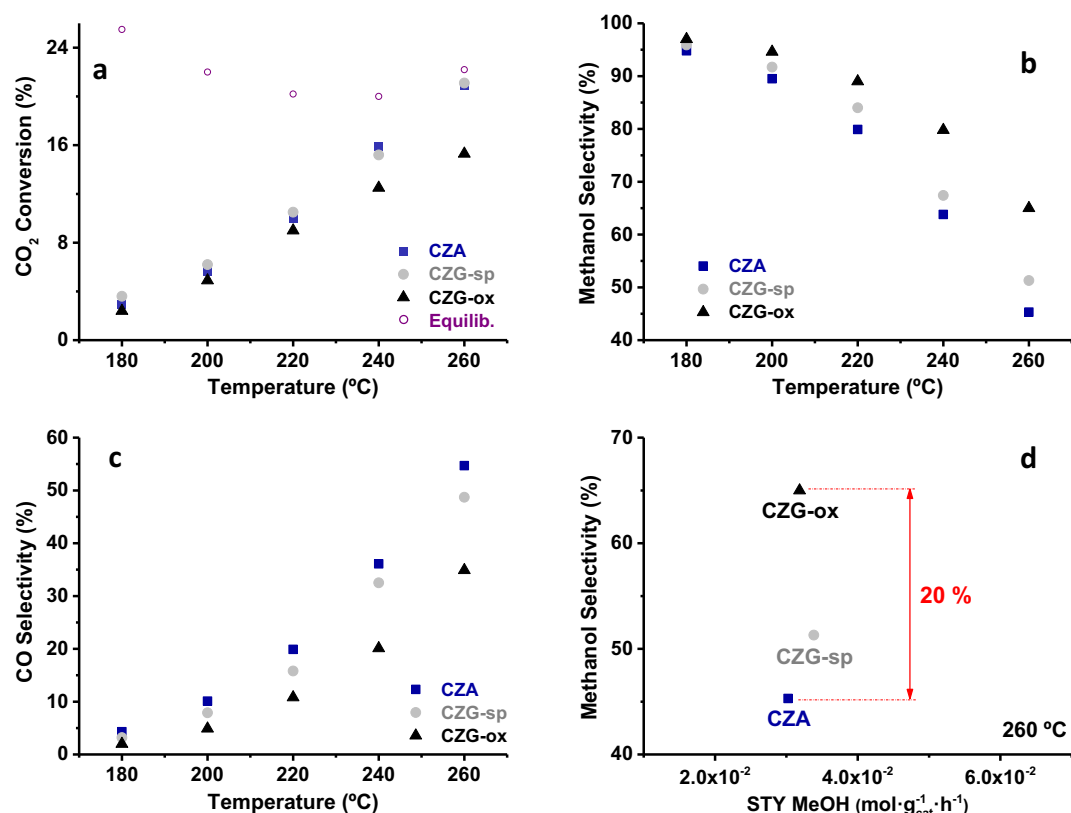
The effect of the Ga loading on the catalytic performance of the most active CZG-ox sample has been studied, with metal loadings between 1 and 7 wt% (details for synthesis and catalytic performance in SI). As shown in Fig. S12 and Table S8 similar methanol production has been obtained at the different Ga loadings in the final catalyst.

### 3.3. Determination of catalytic sites involved in the catalytic performance

In order to understand the effect that the speciation of gallium as promoter has on the properties of active sites, (i.e., copper electronic properties, surface basicity, ZnO decoration, etc.), and trying to correlate them with the catalytic activity of the studied samples, spectroscopic characterization combining state of the art techniques, like near ambient pressure (NAP) XPS and IR of CO as probe molecule, with $TPD-CO_2$ and H_2/D_2 isotopic exchange have been done.

3.3.1. (NAP) XPS

The XPS BE of Cu $2p_{3/2}$, Zn $2p_{3/2}$ and Ga $2p_{3/2}$ core levels acquired at variable sampling depth (between 2.0 and 4.3 nm) and at the different chemical environments (H_2 and CO_2/H_2) (see Experimental Section for more details) correspond in all cases to Cu^0 (Cu $2p_{3/2} \sim 932.2 \pm 0.1$ eV and $CuL_3M_{45}M_{45}$ 919.5 eV), Zn^{2+} (Zn $2p_{3/2} \sim 1021.8 \pm 0.3$ eV) and Ga^{3+} (Ga $2p_{3/2} \sim 1118.0 \pm 0.2$ eV). The corresponding values are included in Tables S9–S11 and the XPS core level displayed in Figs. S13–S15. Those values are similar in all samples and do not demonstrate the differences reflected in the Ga K-edge absorption spectra discussed above. A similar

Table 1
Catalytic results of CZG and CZA samples at 20 bar pressure and at variable temperature (180–260 °C).

T (°C)	Catalyst	X_{CO2} (%)	S_{CO2}, Products (%)			STY ($mol_{prod} \cdot g_{cat}^{-1} \cdot h^{-1}$)		Intrinsic activity ($mol_{prod} \cdot mol_{Cu,s}^{-1} \cdot s^{-1}$)	
			MeOH	CO	HCOOMe	MeOH	CO	MeOH	CO
180	CZA	2.9	94.8	4.3	0.9	$8.78 \cdot 10^{-3}$	$3.98 \cdot 10^{-4}$	$8.76 \cdot 10^{-4}$	$3.97 \cdot 10^{-5}$
	CZG-sp	3.6	95.9	3.2	0.9	$1.08 \cdot 10^{-2}$	$3.60 \cdot 10^{-4}$	$1.26 \cdot 10^{-3}$	$4.20 \cdot 10^{-5}$
	CZG-ox	2.4	97.0	2.0	1.0	$7.46 \cdot 10^{-3}$	$1.54 \cdot 10^{-4}$	$1.63 \cdot 10^{-3}$	$3.36 \cdot 10^{-5}$
200	CZA	5.6	89.5	10.1	0.4	$1.60 \cdot 10^{-2}$	$1.81 \cdot 10^{-3}$	$1.60 \cdot 10^{-3}$	$1.80 \cdot 10^{-4}$
	CZG-sp	6.2	91.7	7.9	0.4	$1.78 \cdot 10^{-2}$	$1.53 \cdot 10^{-3}$	$2.07 \cdot 10^{-3}$	$1.78 \cdot 10^{-4}$
	CZG-ox	4.9	94.6	4.9	0.5	$1.48 \cdot 10^{-2}$	$7.69 \cdot 10^{-4}$	$3.25 \cdot 10^{-3}$	$1.68 \cdot 10^{-4}$
220	CZA	10.0	79.9	19.9	0.2	$2.55 \cdot 10^{-2}$	$6.36 \cdot 10^{-3}$	$2.54 \cdot 10^{-3}$	$6.34 \cdot 10^{-4}$
	CZG-sp	10.5	84.0	15.8	0.2	$2.76 \cdot 10^{-2}$	$5.19 \cdot 10^{-3}$	$3.21 \cdot 10^{-3}$	$6.04 \cdot 10^{-4}$
	CZG-ox	9.0	89.0	10.8	0.2	$2.57 \cdot 10^{-2}$	$3.11 \cdot 10^{-3}$	$5.61 \cdot 10^{-3}$	$6.81 \cdot 10^{-4}$
240	CZA	15.9	63.8	36.1	0.1	$3.24 \cdot 10^{-2}$	$1.83 \cdot 10^{-2}$	$3.23 \cdot 10^{-3}$	$1.83 \cdot 10^{-3}$
	CZG-sp	15.2	67.4	32.5	0.1	$3.20 \cdot 10^{-2}$	$1.55 \cdot 10^{-2}$	$3.73 \cdot 10^{-3}$	$1.80 \cdot 10^{-3}$
	CZG-ox	12.5	79.8	20.1	0.1	$3.19 \cdot 10^{-2}$	$8.05 \cdot 10^{-3}$	$6.99 \cdot 10^{-3}$	$1.76 \cdot 10^{-3}$
260	CZA	20.9	45.3	54.7	0.0	$3.02 \cdot 10^{-2}$	$3.65 \cdot 10^{-2}$	$3.02 \cdot 10^{-3}$	$3.64 \cdot 10^{-3}$
	CZG-sp	21.1	51.3	48.7	0.0	$3.38 \cdot 10^{-2}$	$3.21 \cdot 10^{-2}$	$3.94 \cdot 10^{-3}$	$3.74 \cdot 10^{-3}$
	CZG-ox	15.3	65.0	34.9	0.1	$3.18 \cdot 10^{-2}$	$1.71 \cdot 10^{-2}$	$6.97 \cdot 10^{-3}$	$3.74 \cdot 10^{-3}$

Fig. 4. Selected catalytic features for the CO_2 hydrogenation to MeOH on CZG and CZA samples: CO_2 conversion, including thermodynamic equilibrium (a), MeOH selectivity (b), CO selectivity (c) versus temperature; MeOH selectivity versus space time yield to MeOH at 260 °C (d).
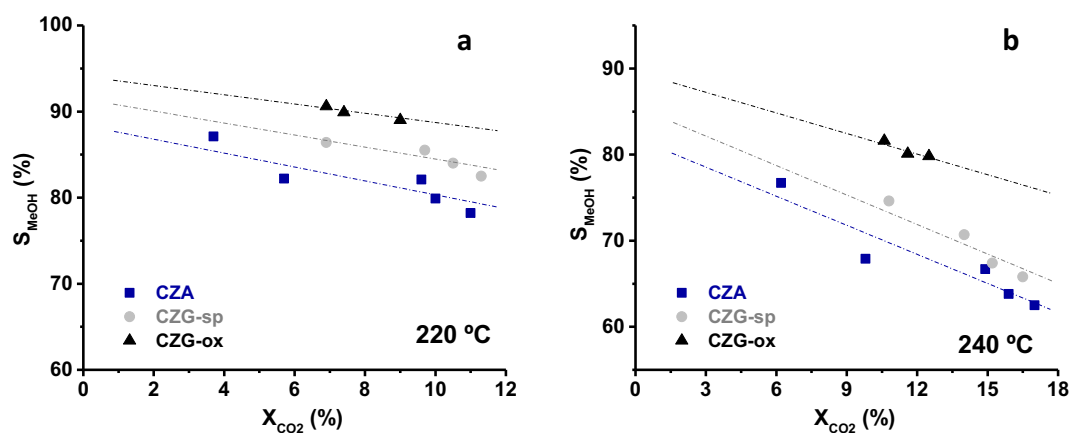

Fig. 5. Variation of the MeOH selectivity versus CO_2 conversion at 220 °C (a) and 240 °C (b).

trend has been observed in previous studies, concluding that the Ga 2p core levels were not sensitive enough to the chemical environment around the atoms [36]. Some authors, specifically in the case of gallium-promoted Cu/ZnO samples, identified a component in the Zn 2p XPS line at 2 eV lower BE than that of ZnO that has been ascribed to Zn^0 species [10,11]. However, identification of Zn^0 by XPS is controversial due to the overlapping of the BE of zinc oxide with Zn^0 [37–41], making those assessments doubtful. Analysis at the O 1s XPS core line acquired at the most surface sensitive conditions (i.e., at low X-ray energy (700 eV), Fig. S16 and Table S12) reveals three components at ~530.6 eV, 531.4 eV and 532.9 eV, corresponding to lattice oxygen "O^{2-}", oxygen vacancies and/or surface hydroxyl groups (–OH) and carbonate species,

respectively [42]. The lower percentage found for the 531.4 eV component corresponds to the CZG-ox sample, in agreement with a less defective structure as determined by EIS measurements.

The surface composition at variable sampling depth in reduced and working catalysts under steady-state conditions is displayed in Fig. 6 for the three samples under different environments. Significant deviation from the nominal composition determined by ICP for all three measured samples is observed (Tables S13–S15), with Zn enrichment at the surface, in agreement with previous results obtained on Cu/ZnO based catalysts [43–46].

According to Fig. 6a, a higher surface coverage of ZnO is observed in the reduced CZG-ox sample compared to the other ones (Fig. 6d for CZG-sp and 6 g for CZA). As consequence, the
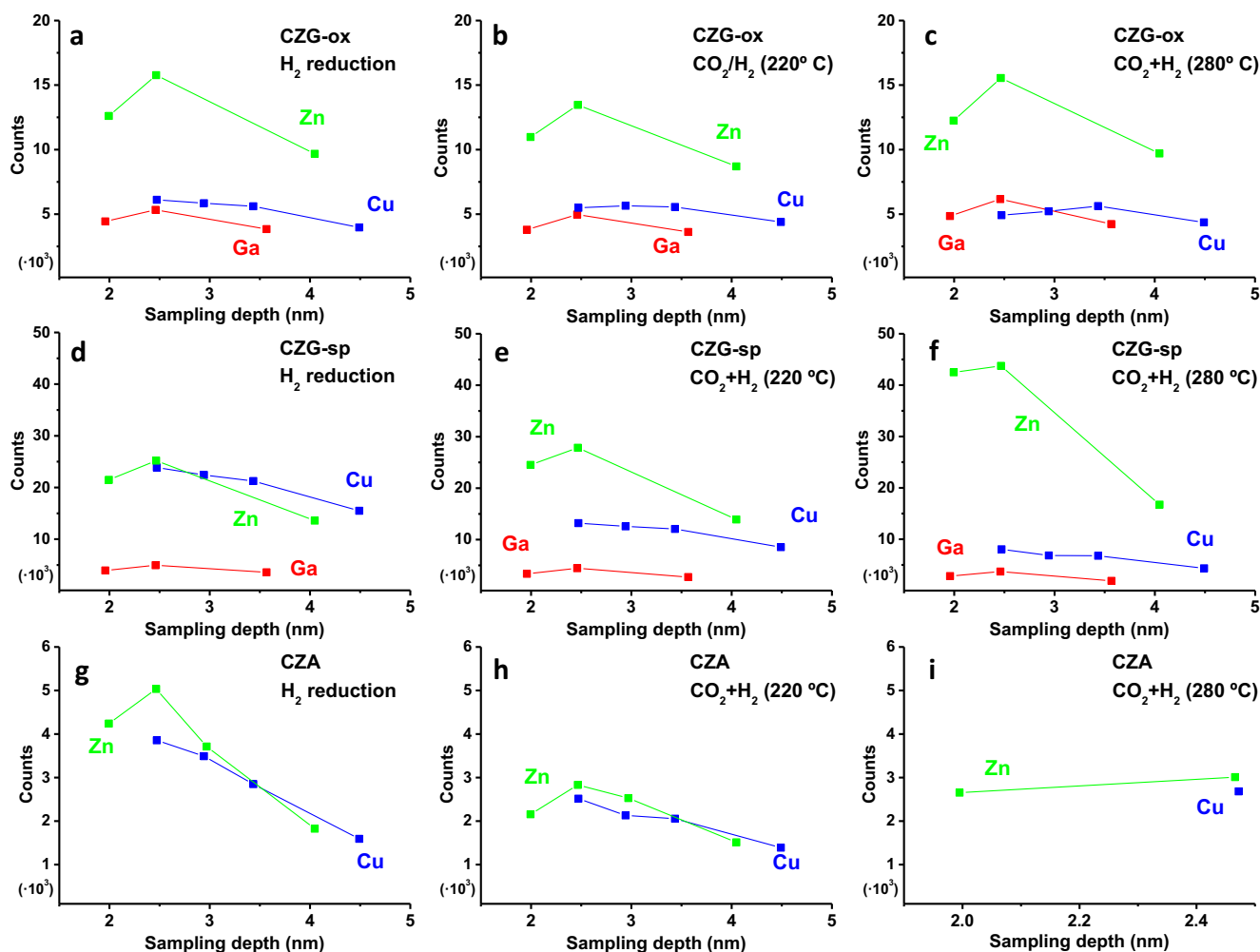
Fig. 6. CZG-ox (a,b,c), CZG-sp (d,e,f) and CZA (g,h,i) XPS depth profile spectra at different reaction conditions. Left: spectra of reduced catalysts. Middle: spectra under $CO_2 + H_2$ atmosphere at 220 °C. Right: spectra under $CO_2 + H_2$ atmosphere at 280 °C.

number of exposed surface Cu sites (SA_{Cu}), determined by N_2O chemisorption (see Table S1) is markedly lower in this sample. The ZnO coverage does not match with the catalyst reducibility (see SI for TPR-H_2 analysis), while should be related to the dissimilar interaction among the precursor phases in the different synthetic methods used in each case. In addition, from XPS depth profile analysis, it can be observed that the distribution of Ga and Zn species with respect to Cu is different in the reduced CZG-sp (Fig. 6d) and CZG-ox samples (Fig. 6a), compared to CZA (Fig. 6g), which may correspond to dissimilar locations and interactions of the different chemical phases within the catalyst. Thus, the stabilization of different copper-metal oxide interfaces, i.e., Cu-Zn (ZnO) in the CZA and CZG-sp samples, and Cu-Ga (Ga^{3+} doped ZnO) in the CZG-ox sample can be predicted. Undoubtedly, the stabilization of different interfaces influences the electronic properties of the adjacent copper sites, as revealed in the next section by IR spectroscopy using CO as probe molecule.

Exposing the catalysts to conditions close to the reaction inside the XPS analysis chamber, i.e., 10 mL·min^{-1} CO_2/H_2 flow at 2.5 mbar, a slight migration of ZnO_x over the Cu NP is observed in the CZG-sp sample at the usual reaction temperatures, i.e., 220 °C (Fig. 6e and Fig. S17a), being more prominent at a higher reaction temperature, i.e., 280 °C (Fig. 6f and Fig. S17b). The dynamic migration of ZnO_x and the redistribution of interfacial sites under reaction conditions are less pronounced in the CZG-

ox (Fig. 6b,c and Fig. S18) and practically not detected in the CZA sample (Fig. 6h,i).

In order to correlate the (NAP) XPS spectroscopic data obtained in the mbar range with the catalytic structural features presented under practical catalytic reaction conditions (i.e., 20 bar), MS analysis of the reaction products in the (NAP) XPS studies has been tracked, together with catalytic studies performed in the flow reactor at lower pressures, i.e., 1 bar, and compared to those at higher pressure, i.e., 20 bar (Fig. S19 and Table S16). As presented in Fig. S20, online MS data show that the formation of methanol (m/z = 32), CO (m/z = 28), and H_2O (m/z = 18) increases with the reaction temperature. Notably, the ratios of CO/CO_2 (m/z = 28/44) and $MeOH/CO_2$ (m/z = 32/44) in the three samples match linearly with the CO and methanol yield obtained at 220 °C and 20 bar in the catalytic flow reactor (see Figure S21).

3.3.2. IR-CO

The electron charge density of surface copper species was analysed by IR spectroscopy using CO as probe molecule. Since the adsorption of CO may cause the reconstruction and sintering of the copper particles [47], the IR adsorption experiments have been done at low temperature (i.e., −50 °C) in this work.

According to the results shown in Fig. 7, different types of copper species are distinguished, characterized by dissimilar CO vibration frequencies. Thus, a band at ~2122 cm^{-1} with a small
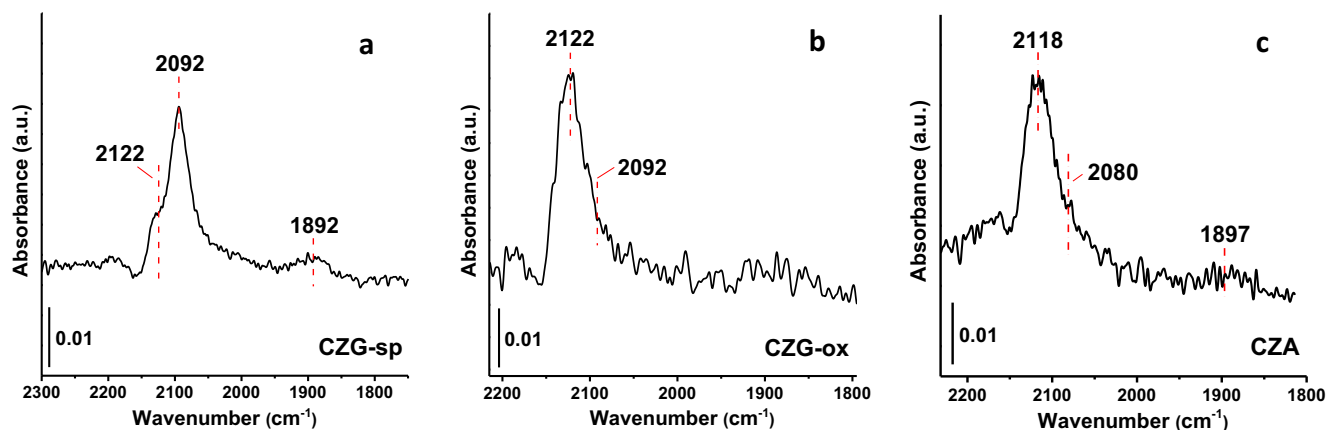
Fig. 7. IR spectra of CO adsorbed at −50 °C on *in situ* reduced CZG-sp, CZG-ox and CZA samples.

shoulder at 2092 cm^{-1} is perceived in the CZG-ox sample. This band is also detected in the CZG-sp sample, in addition to IR bands at 2092 and 1892 cm^{-1}. In the CZA sample, IR bands at 2118, 2080 and 1897 cm^{-1} are observed. IR bands below 2100 cm^{-1} are due to CO adsorption on metallic Cu, where the IR bands at 2092–2080 cm^{-1} are associated to lineal bonded Cu^0-CO on high indexed Cu surface planes, and the 1897–1892 cm^{-1} IR bands to bridging CO species on the Cu(111) surface [48,49]. The IR band at 2118 cm^{-1} is related to copper species, most probably located at the interface to the metal oxide.[48] Regarding the assignation of the IR band at 2122 cm^{-1}, it has been assigned to linear CO species adsorbed on Cu$^+$ [50–53] or to positively charged Cu$^{\delta+}$ [48] or defective Zn$^{\delta+}$. The promoting effect of Ga in stabilizing Cu$^+$ species has already been reported in the literature [14,15]. In fact, the IR band at 2122 cm^{-1} is only observed in the gallium promoted samples. Interestingly, metallic copper is detected in minor extent in the CZG-ox sample, which remarkably shows a strong CO inhibiting effect in the catalytic studies. Assuming that copper species, as Cu^0, are involved in the activation of H$_2$, this raises a considerable distrust about the effective activation of H$_2$ in the CZG-ox sample. In order to answer this question, H$_2$-D$_2$ isotopic exchange experiments were performed, showing similar exchange ability in all samples (Fig. 8).
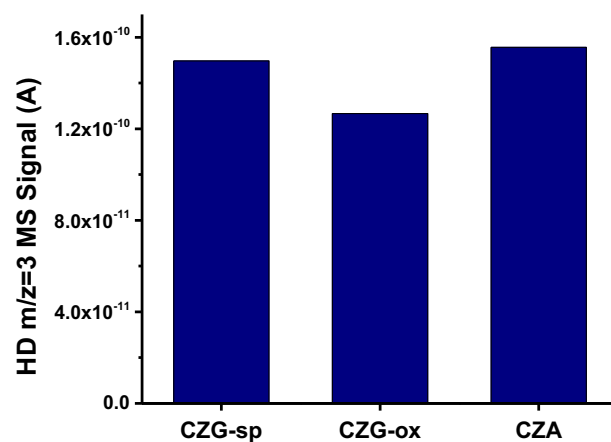
3.3.3. TPD-CO$_2$

Surface basic sites have been proposed in several studies to play an important role in the stabilization of different reaction intermediate species, being moderate basic sites [54–57] that are critical for enhanced methanol selectivity. Indeed, some authors found a lineal correlation [16,54,55] between the amount of basic sites and methanol selectivity. In this regard, TPD-CO$_2$ analysis has been performed, and the corresponding TPD patterns of the herein studied catalysts are displayed in Fig. 9, and that of reference samples (i.e., ZnO, ZnGa$_2$O$_4$, CuGa$_2$O$_4$ and Ga$_2$O$_3$) in Fig. S28.

Three different regions are clearly observed: <200 °C, 200–400 °C and >400 °C. At low temperature (<200 °C), a peak around 80 °C is distinguished in all samples, ascribed to weakly interacting CO$_2$ molecules with surface hydroxyl groups. On the other hand, desorption peaks above 400 °C may not contribute to the catalytic activity due to the high interaction strength with the catalyst surface, and can be considered as spectator species. Therefore, only desorption peaks in the 200–400 °C range can be considered as relevant for the catalytic process, being ascribed to metal–oxygen pairs, surface defects and low coordinated oxygen anions [55,56]. In fact, it is in this temperature range where the main differences between catalysts are observed, revealing different nature of basic sites (Fig. 9). The amount of basic sites increases in the studied cat-
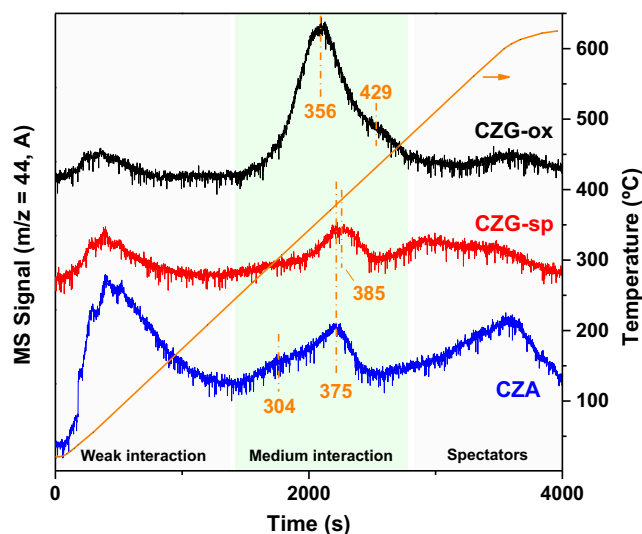

Fig. 8. H$_2$-D$_2$ isotopic exchange results for CZG and CZA samples at 90 °C.

Fig. 9. TPD-CO$_2$ experiments performed on CZG and CZA catalysts.

alysts compared to that of the reference samples (Fig. S28), where the highest CO$_2$ desorption is observed in the CZG-ox sample (Table S18). In addition, a different desorption pattern is observed in this sample, with a desorption peak at 356 °C, slightly lower than that in the CZG-sp and CZA samples (with maxima at

~375–385 °C). In fact, NAP (XPS) shows a highest amount of surface metal oxide decorating the Cu NP in the CZG-ox sample, which may account for a higher number of surface basic sites.

3.4. Determination of structure–activity correlations

In the CO_2 hydrogenation to methanol many intercorrelated parameters are usually involved, making a clear distinction of the active component difficult. That is the reason why a multimodal approach is necessary in order to address the complexity of commercial-like catalysts. In our study, Ga^{3+}-doped ZnO has been shown as a more efficient promoter than $ZnGa_2O_4$, enhancing methanol selectivity versus CO formation. Different spectroscopic tools have been used in order to unveil the reason behing this promoting effect. It is shown that the presence of gallium increases the conductivity of the catalysts, behaving both CZG-ox and CZG-sp as n-type semiconductors. The concentration of surface defects is higher in the CZG-sp sample (containing $ZnGa_2O_4$) than in the Ga^{3+}-doped ZnO sample (i.e., CZG-ox). In the CZG-sp sample, the presence of surface vacancies (i.e., defects) with loosely bounded electrons increases the conductivity of the material. These defects have been considered as active sites in CO_2 activation. Nevertheless, surface basicity, as discussed later, is important for the stabilization of intermediate species, directing the selectivity of the reaction. In our work, a higher concentration of moderate surface basicity is observed in the Ga^{3+}-doped ZnO sample, (i.e., CZG-ox), compared to the other samples, behaving this as the most selective sample.

In addition, based on depth profile XPS studies, different interfaces are visualized among the samples, being the copper-gallium interaction favoured in the CZG-ox sample. In agreement with other studies, the gallium interface stabilize $Cu^{+/\delta+}$ ions, which are observed using IR of CO as probe molecule in both gallium promoted samples. The stabilization of $Cu^{+/\delta+}$ species boosting methanol synthesis has been reported by several authors [12–16], and agrees with the higher selectivity to methanol observed on both CZG-sp and CZG-ox samples, compared with the CZA one. Interestingly, metallic copper surface species (Cu^0) appears as a minor component in the IR studies of the CZG-ox sample. This material exhibits the highest intrinsic activity if methanol production is normalized to the exposed copper surface area determined by N_2O, which may indicate a different nature of active sites, either at the copper particle or at copper interfacial sites. In particular, depth profile XPS studies show a high surface coverage with zinc oxide species in the CZG-ox sample, which explains the higher number of surface exposed basic sites observed from TPD-CO_2 studies. Moreover, while it has been generally reported that the presence of dopants in metal oxide lattice modify its surface acid/base properties [58–60], we cannot confirm at this state if Ga^{3+} doping contributes to the acid/base properties of the ZnO support, but we can safely assess that the density of surface sites with moderate basicity has increased compared to the rest of the samples and the pure ZnO. In a recent work of Bonura et al., the methanol formation rate has been discussed as a function of the N_2O/CO_2 ratio [61]. This parameter represents the extent of metal and oxide surface sites, where a balanced amount of both sites has been proposed to promote methanol production. In our case, methanol production is shown to be sensitive to the number of surface basic sites (see Fig. S29), being enhanced at increasing the number of moderate surface basic centers. This result indicates the importance of surface basic sites in CO_2 activation, in agreement with previous studies in the literature [57–60]. Moreover the lower amount of surface metallic copper determined by IR-CO in the CZG-ox may also contribute to the inhibiting effect of CO formation, where metallic copper has been correlated by several authors with the CO production by the RWGS reaction [18,62,63].

3.5. Application at large scale: opportunities and limitations

Progress in the thermo-catalytic CO_2 reduction through innovative design of new catalysts and process engineering are important aspects in order to accelerate and expand the deployment of these technologies in a circular carbon economy market. In this work we studied a new type of gallium promoted copper-based catalyst containing Ga^{3+}-doped ZnO species. We found a promoting effect in methanol production on Ga^{3+}-doped ZnO copper-based catalysts, compared to a reference catalyst containing $ZnGa_2O_4$ phase and the commercial $Cu/ZnO/Al_2O_3$ catalyst. The CZG-ox system looks promising, with enhanced methanol selectivity, specifically at conditions where the RWGS starts to predominate (260 °C), but it is limited by its low surface area, reducing its activity. In this direction, further studies are ongoing in order to improve the physico-chemical characteristics that definitely affects the methanol production. Despite of it, the catalyst compares well with the most active ones reported in the literature (as already discussed in Fig. S11).

Another important parameter for its application at large scale is the long-term stability under reaction conditions. In this sense, catalytic studies over 100 h time on stream have been performed at 240 °C, 20 bar and at a space velocity (WHSV) of 28500 mL·g_{cat}^{-1}·h^{-1}, on the CZG-ox and compared to the commercial-like CZA sample (Fig. 10). On both catalysts, a decrease in methanol production is mainly observed in the first ~25 h, remaining then practically stable until the rest of the experiment. The initial decrease in
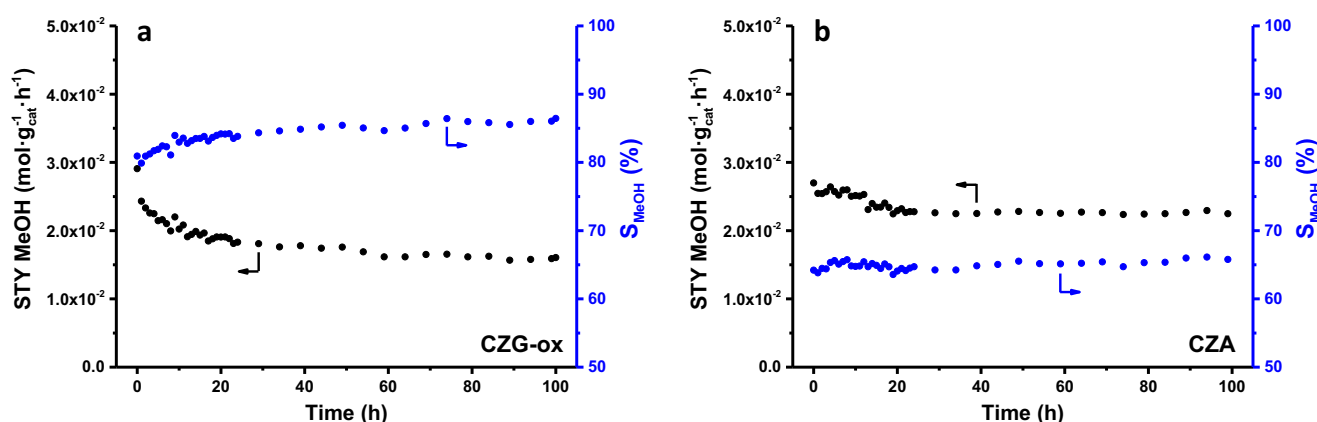

Fig. 10. Long-term experiments conducted on CZG-ox and the commercial CZA samples at 240 °C, 20 bar and 28500 mL·g_{cat}^{-1}·h^{-1}.

methanol production is higher in the CZG-ox sample (~38%) than in the CZA one (~16%). This has been usually ascribed to sintering of the copper nanoparticles due to water formation under reaction conditions or due to poisoning of active sites by water adsorption. The XRD analysis of the samples prior and after reaction are shown in Fig. S4b and Table S2, revealing slight change in crystal size. Since the addition of Al_2O_3 has been reported to enhance catalyst stability, a preliminary study has been done on the CZG-ox sample adding 12.5 % wt ratio Al_2O_3 (details of the synthesis can be found in the experimental section placed in the SI, labelled as CZGA-ox). As verified in Fig. S30a an improvement in the catalyst stability is observed, while keeping similar selectivity pattern as in the original CZG-ox sample (Fig. S30b). Further studies are ongoing, which will be discussed in a future work.

In addition, the scalability of the synthesis method has been studied by synthesizing two additional batches with a final yield of 6.48 g (CZG-ox-2) and 9.61 g (CZG-ox-3), (more details in Section 9 of the SI). The catalytic performance of both batches remains relatively similar to that of the reference CZG-ox catalyst, maintaining a 84–90% of the original activity in CZG-ox-2 and 80–84% in CZG-ox-3 at different temperatures (Figs. S32a and S33), and keeping similar selectivity pattern as in the reference sample (Fig. S32b).

4. Conclusions

In conclusion, the promoting effect of gallium on the structural, electronic and catalytic properties of two selected $CuO/ZnO/Ga_2O_3$ catalysts in the methanol synthesis from CO_2 hydrogenation has been studied in this work. Although the promoting effect of Ga has been subject of many research papers, Ga^{3+}-doped wurtzite ZnO has been scarcely studied in the methanol synthesis reaction. In addition, a deeper understanding of the promoting underlaying mechanism and interactions among the active components will help in uncovering the complexity of industrial-like Cu/ZnO catalysts, requesting a multimodal spectroscopic-catalytic approach. In this work, we found that Ga^{3+}-doped in ZnO is a more effective promoter than the already reported $ZnGa_2O_4$ phase. The speciation of gallium can be controlled by simply changing the precipitating agent during the coprecipitation of the metal precursors, keeping the rest variables constant. Thus, Ga^{3+}-doped ZnO is formed by coprecipitating with NaOH, while $ZnGa_2O_4$ appears by using NH_4-HCO_3. Compared to the reference $Cu/ZnO/Al_2O_3$ (CZA) catalyst, an inhibition of CO formation and enhanced methanol production is observed in the gallium promoted samples and, in particular, in the one characterised by the presence of Ga^{3+}-doped ZnO domains (CZG-ox). Long-term catalytic test over 100 h time on stream shown a decrease in methanol production of ~38% in the first 25 h of reaction, remaining constant until the end of the experiment. This value is higher than that observed in the commercial $Cu/ZnO/Al_2O_3$ (CZA) catalyst, where Al_2O_3 behaves as a structural promoter. In fact, adding 12.5 % Al_2O_3 to the CZG-ox catalyst results in a less marked catalyst deactivation. On the other hand, a fairly good scalability of the synthesis approach has been observed up to 10 g, with ~15% activity loss, while maintaining similar selectivity pattern as in the reference CZG-ox sample.

As a result of our work, a complex scenario where both the electrochemical potential of the sample and the structural properties of the catalyst are mutually influenced, underlining the need for a multidisciplinary spectroscopic approach for accurate catalytic characterization.

Finally, the promoting effect of Ga^{3+}-doped ZnO wurtzite phase for enhanced methanol synthesis found in this work may open new perspectives in the design of novel catalytic systems with tailored interfaces, not only in thermal, but also in photo/electro reduction of carbon dioxide. However, further studies are needed in order to be competitive for industrial applications.

CRediT authorship contribution statement

Jorge Cored: Conceptualization, Visualization, Formal analysis, Investigation, Writing – original draft. **Christian Wittee Lopes:** Methodology, Formal analysis, Investigation, Writing – original draft. **Lichen Liu:** Formal analysis, Investigation, Writing – original draft. **Jose Soriano:** Investigation. **Giovanni Agostini:** Funding acquisition, Writing – original draft, Methodology, Formal analysis, Investigation, Resources. **Benjamín Solsona:** Methodology, Investigation. **Rita Sánchez-Tovar:** Formal analysis, Methodology, Investigation. **Patricia Concepción:** Conceptualization, Methodology, Formal analysis, Investigation, Resources, Writing – review & editing, Visualization, Supervision, Funding acquisition.

Declaration of Competing Interest

The authors declare that they have no known competing financial interests or personal relationships that could have appeared to influence the work reported in this paper.

Appendix A. Supplementary material

Supporting Information includes synthetic details of samples and reference materials; Characterization techniques; Physicochemical properties of the catalysts; XRD characterization; EXAFS characterization; Electrical properties; Catalytic properties; State of art in methanol synthesis; (NAP)-XPS experiments at Bessy II (Berlin); Influence of pressure in the CO_2 hydrogenation reactor; Laboratory scale XPS studies; $TPD-CO_2$; Long-term experiments, Scalability of the synthetic procedure. Supplementary data to this article can be found online at https://doi.org/10.1016/j.jcat.2022.01.032.

References

[1] D. Sheldon, Methanol production – a technical history, Johnson Matthey Technol. Rev. 61 (2017) 172–182.

[2] N. Meunier, R. Chauvy, S. Mouhoubi, D. Thomas, G. De Weireld, Alternative production of methanol from industrial CO_2, Renew. Energy 146 (2020) 1192–1203.

[3] B. Liang, J. Ma, X. Su, C. Yang, H. Duan, H. Zhou, S. Deng, L. Li, Y. Huang, Investigation on Deactivation of $Cu/ZnO/Al_2O_3$ Catalyst for CO_2 Hydrogenation to Methanol, Ind. Eng. Chem. Res. 58 (2019) 9030–9037.

[4] J. Zhong, X. Yang, Z. Wu, B. Liang, Y. Huang, T. Zhang, State of the art and perspectives in heterogeneous catalysis of CO_2 hydrogenation to methanol, Chem. Soc. Rev. 49 (2020) 1385–1413.

[5] G. Centi, E.A. Quadrelli, S. Perathoner, Catalysis for CO_2 conversion: a key technology for rapid introduction of renewable energy in the value chain of chemical industries, Energy Environ. Sci. 6 (2013) 1711–1731.

[6] W. Wang, S. Wang, X. Ma, J. Gong, Recent advances in catalytic hydrogenation of carbon dioxide, Chem. Soc. Rev. 40 (2011) 3703–3727.

[7] A. Goeppert, M. Czaun, J.P. Jones, G.K.S. Prakash, G.A. Olah, Recycling of carbon dioxide to methanol and derived products – closing the loop, Chem. Soc. Rev. 43 (2014) 7995–8048.

[8] S. Kattel, P.J. Ramírez, J.G. Chen, J.A. Rodriguez, P. Liu, Active sites for CO₂ hydrogenation to methanol on Cu/ZnO catalysts, Science 355 (2017) 1296–1299.

[9] S. Natesakhawat, J.W. Lekse, J.P. Baltrus, P.R. Ohodnicki Jr., B.H. Howard, X. Deng, C. Matranga, Active Sites and Structure-Activity Relationships of Copper-Based Catalysts for Carbon Dioxide Hydrogenation to Methanol, ACS. Catal. 2 (2012) 1667–1676.

[10] M.M.J. Li, Z. Zeng, F. Liao, X. Hong, S.C.E. Tsang, Enhanced CO₂ hydrogenation to methanol over CuZn nanoalloy in Ga modified Cu/ZnO catalysts, J. Catal. 343 (2016) 157–167.

[11] M.M.J. Li, C. Chen, T. Ayvali, H. Suo, J. Zheng, I.F. Teixeira, L. Ye, H. Zou, D. O'Hare, S.C.E. Tsang, CO₂ hydrogenation to methanol over catalysts derived from single cationic layer CuZnGa LDH precursors, ACS Catal. 8 (2018) 4390–4401.

[12] M. Saito, T. Fujitani, T. Takeuchi, T. Watanabe, Development of copper/zinc oxide-based multicomponent catalysts for methanol synthesis from carbon dioxide and hydrogen, Appl. Catal. A. 138 (1996) 311–318.

[13] P. Gao, F. Li, F. Xiao, N. Zhao, N. Sun, W. Wei, L. Zhong, Y. Sun, Preparation and activity of Cu/Zn/Al/Zr catalysts via hydrotalcite-containing precursors for methanol synthesis from CO₂ hydrogenation, Catal. Sci. Technol. 2 (2012) 1447–1454.

[14] J. Toyir, P. Ramírez de la Piscina, J.L.G. Fierro, N. Homs, Catalytic performance for CO₂ conversion to methanol of gallium-promoted copper-based catalysts: influence of metallic precursors, Appl. Catal. B 34 (2001) 255–266.

[15] J. Toyir, P. Ramírez de la Piscina, J.L.G. Fierro, N. Homs, Highly effective conversion of CO₂ to methanol over supported and promoted copper-based catalysts: influence of support and promoter, Appl. Catal. B 29 (2001) 207–215.

[16] X. Dong, F. Li, N. Zhao, F. Xiao, J. Wang, Y. Tan, CO₂ hydrogenation to methanol over Cu/ZnO/ZrO₂ catalysts prepared by precipitation-reduction method, Appl. Catal. B 191 (2016) 8–17.

[17] R. Ladera, F.J. Pérez-Alonso, J.M. González-Carballo, M. Ojeda, S. Rojas, J.L.G. Fierro, Catalytic valorization of CO₂ via metanol synthesis with Ga-promoted Cu-ZnO-ZrO₂ catalysts, Appl. Catal. B: Environ 142–143 (2013) 241–248.

[18] J.C. Medina, M. Figueroa, R. Manrique, J.R. Pereira, P.D. Srinivasan, J.J. Bravo-Suárez, V.G. Baldovino-Medrano, R. Jiménez, A. Karelovic, Catalytic consequences of Ga promotion on Cu for CO₂ hydrogenation to methanol, Catal. Sci. Technol. 7 (2017) 3375–3387.

[19] M. Behrens, S. Zander, P. Kurr, N. Jacobsen, J. Senker, G. Koch, T. Ressler, R.W. Fischer, R. Schlögl, Performance improvement of nanocatalysts by promoter-induced defects in the support material: methanol synthesis over CU/ZnO:Al, J. Am. Chem. Soc. 135 (2013) 6061–6068.

[20] P.K. Mishra, S. Ayaz, T. Srivastava, S. Tiwari, R. Meena, B. Kissinquinker, S. Biring, S. Sen, Role of Ga-substitution in ZnO on defect states, carrier density, mobility and UV sensing, J. Mater. Sci.: Mater. Electron. 30 (2019) 18686–21869.

[21] F. Liao, B.T.W. Lo, E. Tsang, The applications of nano-hetero-junction in optical and thermal catalysis, Eur. J. Inorg. Chem. 2016 (13–14) (2016) 1924–1938.

[22] C. Baltes, S. Vukojevic, F. Schüth, Correlations between synthesis, precursor, and catalyst structure and activity of a large set of CuO/ZnO/Al₂O₃ catalysts for methanol synthesis, J. Catal. 258 (2008) 334–344.

[23] O. Hinrichsen, T. Genger, M. Muhler, Chemisorption of N₂O and H₂ for the surface determination of copper catalysts, Chem. Eng. Technol. 23 (2000) 956–959.

[24] L. Simonelli, C. Marini, W. Olszewski, M. Ávila Pérez, N. Ramanan, G. Guilera, V. Cuarteto, K. Klementiev, N.L. Saini, CLAESS: The hard X-ray absorption beamline of the ALBA CELLS synchrotron, Cogent Phys. 3 (2016) 1231987.

[25] B. Ravel, M. Newville, ATHENA, ARTEMIS, HEPHAESTUS: data analysis for X-ray absorption spectroscopy using IFEFFIT, J. Synchrotron Radiat. 12 (4) (2005) 537–541.

[26] S. Tougaard, QUASES: software packages to characterize surface nanostructures by analysis of electron spectra, <http://www.quases.com/products/quases-imfp-tpp2m/>.

[27] R. Guil-López, N. Mota, J. Llorente, E. Millán, B. Pawelec, R. García, J.L.G. Fierro, R.M. Navarro, Structure and activity of Cu/ZnO catalysts co-modified with aluminium and gallium for methanol synthesis, Catal. Today 355 (2020) 870–881.

[28] A.A. Tountas, X. Peng, A.V. Tavasoli, P.N. Duchesne, T.L. Dingle, Y. Dong, L. Hurtado, A. Mohan, W. Sun, U. Ulmer, L. Wang, T.E. Wood, C.T. Maravelias, M.M. Sain, G.A. Ozin, Towards solar methanol: past, present, and future, Adv. Sci. 6 (2019) 1801903.

[29] R. Van der Berg, G. Prieto, G. Korpershoek, L.I. Van der Wal, A.J. Van Bunningen, S. Laegsgaard-Jorgensen, P.E. de Jongh, K.P. de Jong, Structure sensitivity of Cu and CuZn catalysts relevant to industrial methanol synthesis, Nat. Commun. 7 (2016) 13057.

[30] V.B.R. Boppana, D.J. Doren, R.F. Lobo, Analysis of Ga coordination environment in novel spinel zinc gallium oxy-nitride photocatalysts, J. Mater. Chem. 20 (2010) 9787–9797.

[31] J.A. Sans, G. Martínez-Criado, J. Pellicer-Porres, J.F. Sánchez-Royo, A. Segura, Thermal instability of electrically active centers in heavily Ga-doped ZnO thin films: X-ray absorption study of the Ga-site configuration, Appl. Phys. Lett. 91 (2007) 221904.

[32] M.J. Ward, W.Q. Han, T.K. Sham, 2D XAFS-XEOL mapping of Ga₁₋ₓZnₓN₁₋ₓOₓ nanostructured solid solutions, J. Phys. Chem. C 115 (2011) 20507–20514.

[33] S.S. Shinde, P.S. Shinde, Y.W. Oh, D. Haranath, C.H. Bhosale, K.Y. Rajpure, Structural, optoelectronic, luminescence and thermal properties of Ga-doped zinc oxide thin films, Appl. Surf. Sci. 258 (2012) 9969–9976.

[34] J.D. Ye, S.L. Gu, S.M. Zhu, S.M. Liu, Y.D. Zheng, R. Zhang, Y. Shi, H.Q. Yu, Y.D. Ye, Gallium doping dependence of single-crystal n-type ZnO grown by metal organic chemical vapor deposition, J. Cryst. Growth. 283 (2005) 279–285.

[35] D.T. Phan, G.S. Chung, Effects of defects in Ga-doped ZnO nanorods formed by a hydrothermal method on CO sensing properties, Sensor Actuat. B: Chem. 187 (2013) 191–197.

[36] S. Turczyniak, W. Luo, V. Papaefthimiou, N.S. Ramgir, M. Haevecker, A. Machocki, S. Zafeiratos, A comparative ambient pressure X-ray photoelectron and absorption spectroscopy study of various cobalt-based catalysts in reactive atmospheres, Top. Catal. 59 (2016) 532–542.

[37] M.C. Biesinger, L.W.M. Lau, A.R. Gerson, R.St.C. Smart, Resolving surface chemical states in XPS analysis of first row transition metals, oxides and hydroxides: Sc, Ti, V, Cu and Zn, Appl. Surf. Sci. 257 (2010) 887–898.

[38] C. Wöll, The chemistry and physics of zinc oxide surfaces, Prog. Surf. Sci. 82 (2007) 55–120.

[39] Y. Wang, S. Kattel, W. Gao, K. Li, P. Liu, J.G. Chen, H. Wang, Exploring the ternary interactions in Cu-ZnO-ZrO₂ catalysts for efficient CO₂ hydrogenation to methanol, Nat. Commun. 10 (2019) 1166.

[40] S. Kuld, C. Conradsen, P.G. Moses, I. Chorkendorff, J. Sehested, Quantification of zinc atoms in a surface alloy on copper in an industrial-type methanol synthesis catalyst, Angew. Chem. Int. Ed. 53 (2014) 5941–5945.

[41] V. Schott, H. Oberhofer, A. Birkner, M. Xu, Y. Wang, M. Muhler, K. Reuter, C. Wöll, Chemical activity of thin oxide layers: strong interactions with the support yield a new thin-film phase of ZnO, Angew. Chem. Int. Ed. 52 (2013) 11925–11929.

[42] J.C. Dupin, D. Gonbeau, P. Vinatier, A. Levasseur, Systematic XPS studies of metal oxides, hydroxides and peroxides, Phys. Chem. Chem. Phys. 2 (2000) 1319–1324.

[43] M. Behrens, F. Studt, I. Kasatkin, S. Kühl, M. Hävecker, F. Abild-Pedersen, S. Zander, F. Girgsdies, P. Kurr, B.L. Kniep, M. Tovar, R.W. Fischer, J.K. Norskov, R. Schlögl, The active site of methanol synthesis over Cu/ZnO/Al₂O₃ industrial catalysts, Science 336 (2012) 893–897.

[44] S. Zander, E.L. Kunkes, M.E. Schuster, J. Schumann, G. Weinberg, D. Teschner, N. Jacobsen, R. Schlögl, M. Behrens, The role of the oxide component in the development of copper composite catalysts for methanol synthesis, Angew. Chem. Int. Ed. 52 (2013) 6536–6540.

[45] W.P.A. Jansen, J. Beckers, J.C.V.D. Heuvel, V.D. Denier, A.W. Gon, A. Bliek, H.H. Brongersma, Dynamic behavior of the surface structure of Cu/ZnO/SiO₂ catalysts, J. Catal. 210 (2002) 229–236.

[46] J. Sloczynski, R. Grabowski, P. Olszewski, A. Kozlowska, J. Stoch, M. Lachowska, J. Skrzypek, Effect of metal oxide additives on the activity and stability of Cu/ZnO/ZrO₂ catalysts in the synthesis of methanol from CO₂ and H₂, Appl. Catal. A 310 (2006) 127–137.

[47] A.E. Baber, F. Xu, F. Dvorak, K. Mudiyanselage, M. Soldemo, J. Weissenrieder, S.D. Senanayake, J.T. Sadowski, J.A. Rodriguez, V. Matolín, M.G. White, D.J. Stacchiola, In situ imaging of Cu₂O under reducing conditions: formation of metallic fronts by mass transfer, J. Am. Chem. Soc. 135 (2013) 16781–16784.

[48] J. Schumann, J. Kröhnert, E. Frei, R. Schlögl, A. Trunschke, IR-spectroscopic study on the interface of Cu-based methanol synthesis catalysts: evidence for the formation of a ZnO overlayer, Top. Catal. 60 (2017) 1735–1743.

[49] N.Y. Topsoe, H. Topsoe, On the nature of surface structural changes in Cu/ZnO methanol synthesis catalysts, Top. Catal. 8 (1999) 267–270.

[50] P.B. Sanguineti, M.A. Baltanás, A.L. Bonivardi, Copper-gallia interaction in Cu-Ga₂O₃-ZrO₂ catalysts for methanol production from carbon oxide(s) hydrogenation, Appl. Catal. A 504 (2015) 476–481.

[51] D.B. Clarke, I. Suzuki, A.T. Bell, An infrared study of the interactions of CO and CO₂ with Cu/SiO₂, J. Catal. 142 (1993) 27–36.

[52] F. Xu, K. Mudiyanselage, A.E. Baber, M. Soldemo, J. Weissenrieder, M.G. White, D.J. Stacchiola, Redox-mediated reconstruction of copper during carbon monoxide oxidation, J. Phys. Chem. C 118 (2014) 15902–15909.

[53] O. Dulaurent, X. Courtois, V. Perrichon, D. Bianchi, Heats of adsorption of CO on a Cu/Al₂O₃ catalyst using FTIR spectroscopy at high temperatures and under adsorption equilibrium conditions, J. Phys. Chem. B 104 (2000) 6001–6011.

[54] V.D.B.C. Dasireddy, B. Likozar, The role of copper oxidation state in Cu/ZnO/Al₂O₃ catalysts in CO₂ hydrogenation and methanol productivity, Renew. Energy 140 (2019) 452–460.

[55] S. Chen, J. Zhang, P. Wang, X. Wang, F. Song, Y. Bai, M. Zhang, Y. Wu, H. Xie, Y. Tan, Effect of vapor-phase-treament to CuZnZr catalyst on the reaction behaviors in CO₂ hydrogenation into methanol, Chem. Cat. Chem. 11 (2019) 1448–1457.

[56] P. Gao, F. Li, H. Zhan, N. Zhao, F. Xiao, W. Wei, L. Zhong, H. Wang, Y. Sun, Influence of Zr on the performance of Cu/Zn/Al/Zr catalysts via hydrotalcite-like precursors for CO₂ hydrogenation to methanol, J. Catal. 298 (2013) 51–60.

[57] X. Guo, D. Mao, G. Lu, S. Wang, G. Wu, The influence of La doping on the catalytic behavior of Cu/ZrO₂ for methanol synthesis from CO₂ hydrogenation, J. Mol. Catal. A: Chem. 345 (2011) 60–68.

[58] J.S. Rossi, O.M. Perrone, M.R. Siqueira, D.P. Volanti, E. Gomes, R. Da-Silva, M. Boscolo, Effect of lanthanide ion doping on Mg-Al mixed oxides as active acid-base catalysts for fatty acid ethyl ester synthesis, Renew. Energy 133 (2019) 367–372.

[59] Y. Chen, J. Lin, X. Chen, S. Fan, Y. Zheng, Engineering multicomponent metal-oxide for efficient methane combustion over palladium-based catalysts, Catal. Sci. Technol. 11 (2021) 152–161.

[60] N. Bou-Orm, A. Iorgu, S. Daniele, N. Guilhaume, Modification of acid-base properties of TiO_2 by Nb and Mg dopants: influence on the activity of Pd-Cu/(Mg, Nb)-Ti_O2 catalysts for nitrate hydrogenation, Appl. Catal. A: Gen. 467 (2013) 414–420.

[61] L. Frusteri, C. Cannilla, S. Todaro, F. Frusteri, G. Bonura, Tailoring of hydrotalcite-derived cu-based catalysts for CO_2 hydrogenation to methanol, Catalysts 9 (12) (2019) 1058, https://doi.org/10.3390/catal9121058.

[62] A. Karelovic, G. Galdames, J.C. Medina, C. Yévenes, Y. Barra, R. Jiménez, Mechanism and structure sensitive of methanol synthesis from CO_2 over SiO_2-supported Cu nanoparticles, J. Catal. 369 (2019) 415–426.

[63] Y. Yang, C.A. Mims, R.S. Disselkamp, D. Mei, J.H. Kwak, J. Szanyi, C.H.F. Peden, C.T. Campbell, Isotopic effects in methanol synthesis and the reactivity of copper formates on a Cu/SiO_2 catalyst, Catal. Lett. 125 (2008) 201–208, https://doi.org/10.1007/s10562-008-9592-4.